

Hydrodynamic outcomes of planet scattering in transitional discs

Nickolas Moeckel^{1*} and Philip J. Armitage^{2,3}

¹*Institute of Astronomy, University of Cambridge, Madingley Road, Cambridge, CB3 0HA*

²*JILA, 440 UCB, University of Colorado, Boulder, CO 80309-0440, USA*

³*Department of Astrophysical and Planetary Sciences, University of Colorado, Boulder, USA*

Accepted XXX. Received YYY; in original form ZZZ

ABSTRACT

A significant fraction of unstable multiple planet systems are likely to scatter during the transitional disc phase as gas damping becomes ineffectual. Using a large ensemble of FARGO hydrodynamic simulations and MERCURY n -body integrations, we directly follow the dynamics of planet-disc and planet-planet interactions through the clearing phase and on through 50 Myr of planetary system evolution. Disc clearing is assumed to occur as a result of X-ray driven photoevaporation. We find that the hydrodynamic evolution of individual scattering systems is complex, and can involve phases in which massive planets orbit within eccentric gaps, or accrete directly from the disc without a gap. Comparing the results to a reference gas-free model, we find that the n -body dynamics and hydrodynamics of scattering into one- and two-planet final states are almost identical. The eccentricity distributions in these channels are almost unaltered by the presence of gas. The hydrodynamic simulations, however, also form a population of low eccentricity three-planet systems in long-term stable configurations, which are not found in n -body runs. The admixture of these systems results in modestly lower eccentricities in hydrodynamic as opposed to gas-free simulations. The precise incidence of these three-planet systems is likely a function of the initial conditions; different planet setups (number or spacing) may change the quantitative character of this result. We analyze the properties of surviving multiple planet systems, and show that only a small fraction (a few percent) enter mean-motion resonances after scattering, while a larger fraction form stable resonant chains and avoid scattering entirely. Our results remain consistent with the hypothesis that exoplanet eccentricity results from scattering, though the detailed agreement between observations and gas-free simulation results is likely coincidental. We discuss the prospects for further tests of scattering models by observing planets or non-axisymmetric gas structure in transitional discs.

Key words: planets and satellites: dynamical evolution and stability — planet-disc interactions — planetary systems — protoplanetary discs — hydrodynamics — scattering

1 INTRODUCTION

Prior to gap opening, gravitational interactions between planets and their surrounding gas discs act to efficiently damp planetary eccentricity. This damping implies that the formation of giant planets via core accretion leads to initially circular orbits, and that post-formation dynamical effects must be sought to explain the observed eccentricity distribution of massive extrasolar planets (Butler et al. 2006). Dynamical instability in multi-planet systems, leading to

orbit crossing and the ejection or merger of some of the planets, is one way to achieve this (Rasio & Ford 1996; Weidenschilling & Marzari 1996; Lin & Ida 1997). Extensive n -body experiments have shown that with realistic mass functions, the dynamics of unstable two-planet (Ford & Rasio 2008), three-planet (Chatterjee et al. 2008), or richer systems (Jurić & Tremaine 2008) can successfully reproduce the observed eccentricity distribution.

The good agreement between n -body dynamical experiments and observations is somewhat surprising, as it is hard to envisage a consistent scattering scenario in which gas disc interactions are not important. The simplest model is one

* E-mail: moeckel@ast.cam.ac.uk

in which the typical planetary system forms with just two massive planets. In this case, the only unstable systems have planets that are separated by less than the threshold for Hill stability (Marchal & Bozis 1982; Gladman 1993), and most of the unstable subset scatter on a time scale that is much shorter than the gas disc dispersal time ($\sim 10^5$ yr Wolk & Walter 1996). Scattering is therefore likely to occur as soon as gas disc damping declines below some threshold level, and will be synchronized with the epoch of disc dispersal. Related arguments apply, less robustly, to richer planetary systems. For more than two planets there is no analytic criterion for stability, and relatively loosely packed initial configurations can delay the onset of scattering for tens or hundreds of Myr (Chatterjee et al. 2008). Absent fine tuning, however, it is not possible to construct initial conditions in which *all* of the instabilities occur on $>$ Myr time scales, without over-producing stable low eccentricity systems that are not seen observationally. As the gas dissipates there should therefore be a significant number of systems primed to go unstable, scattering in the presence of at least some remnant gas.

The large computational cost of hydrodynamics relative to gravity has necessarily motivated approximate approaches that marry disc physics to n -body simulations of scattering. One method is to include an analytic description of planet-disc interactions as a force within an n -body calculation. This has been used to study the migration of planets into resonance (e.g. Lee & Peale 2002; Snellgrove et al. 2001), and through resonance into scattering (Adams & Laughlin 2003; Moorhead & Adams 2005; Lee et al. 2009). Scattering with more than two planets in an embedding disc has been studied by Chatterjee et al. (2008) and Matsumura et al. (2010), with the disc modeled in 1D and torques on the planets calculated from that density profile. There have also been preliminary studies that include a full hydrodynamic treatment of the gas disc during active periods of planet scattering. Moeckel et al. (2008) performed 3D simulations starting from very unstable equal-mass, two-planet systems with a remnant gas disc exterior to the planets' orbits. Marzari et al. (2010) performed 2D simulations studying migration and resonant trapping in three-planet systems, some of which led naturally to scattering when resonance was broken. While both of these studies hinted at possibly significant dynamical effects mediated by the gas, they were too limited in scope to attempt statistical comparison to gas-free results.

Our goal in this work is to directly quantify the impact of residual gas discs on the outcome of planet scattering. We assume that the interesting dynamics is coincident with the epoch of disc dispersal, and follow the planet-planet and planet-disc interactions through this transition phase using a 2D hydrodynamic code. We consider three-planet systems, setup almost identically to previous gas-free calculations (Chatterjee et al. 2008; Raymond et al. 2010), and model disc dispersal using a physically motivated photoevaporation model (Owen et al. 2011). The hydrodynamics are run long enough to take the systems through the transition phase into the pure n -body regime, after which we switch to a standard integrator for a further 50 Myr of gravitational interactions.

2 THE SIMULATIONS

2.1 Initial conditions

To facilitate direct comparison with previous n -body results, we consider three-planet systems around stars with mass $M_\star = 1 M_\odot$, with the mass m of each planet drawn randomly from a power law distribution $f(m) \propto m^{-1.1}$ in the range $0.3\text{--}5 M_J$. The innermost planet is placed with a semi-major axis $a_1 = 3$ au, and the spacing of the other planets is determined following the approach of Chambers et al. (1996), with each adjacent planetary pair separated by a fixed number of mutual Hill radii R_{Hij} . That is, with

$$R_{Hij} = \left(\frac{m_i + m_j}{3M_\star} \right)^{1/3} \frac{a_i + a_j}{2}, \quad (1)$$

the middle planet is placed at $a_2 = a_1 + KR_{H12}$, and the outer planet at $a_3 = a_2 + KR_{H23}$. The constant K largely determines the timescale on which gravitational instability occurs (Chambers et al. 1996; Marzari & Weidenschilling 2002; Chatterjee et al. 2008). We set K at approximately the maximum value that does not overproduce stable systems, whose low final eccentricity would be inconsistent with exoplanet observations. With our mass spectrum, experimentation showed that $K = 4.0$ yielded a distribution of instability times with a median $t_i \sim 4 \times 10^4$ yr, and $\sim 10\%$ of the setups unscattered after 50 Myr¹.

The planets are initially embedded in a gas disc which we model between 1 and 40 au. The surface density initially follows a radial profile $\Sigma(r) = 200 (r/1 \text{ au})^{-1} \text{ g cm}^{-2}$. We include photoevaporation of the disc using the mass-loss profiles of Owen et al. (2011), which are based on the coupled hydrodynamic and radiative transfer models introduced by Owen et al. (2010). In these models, X-ray luminosity drives photoevaporative disc dispersal. Our discs initially contain just over $5 M_J$ of gas, which is both the typical total mass of the three planets and the mass at which the photoevaporative mass loss begins to alter the disc structure on a fast timescale. We pragmatically set the X-ray luminosity of our star at $1.4 \times 10^{30} \text{ erg s}^{-1}$, which yields a disc clearing timescale of just over 10^5 years depending on the details of the planet-disc interactions (see Figure 1). This timescale, coupled with our chosen planet spacing, means that about half our systems might be expected to scatter when there is still a significant amount of disc material left.

We evolve 100 random realizations of the planetary initial conditions within the fixed initial conditions for the disc. We use direct hydrodynamic simulations to model the coupled planetary and disc dynamics while the disc mass is high enough to still influence the planets' evolution, followed by a longer n -body run once the disc has been cleared. For the hydrodynamic portion of each run we use a modified version of the 2D code FARGO (Masset 2000), and for the n -body follow-on we use MERCURY (Chambers 1999).

FARGO is a 2D Eulerian hydrodynamic code tailored to

¹ This instability timescale is about an order of magnitude larger than the result for $K = 4.0$ with equal mass planets found by Chatterjee et al. (2008), where for a given K each planetary pair is at a fixed separation relative to the major mean motion resonances. With our mass spectrum and $K = 4$, each adjacent pair is somewhere between roughly the 3:2 and 2:1 mean motion resonances.

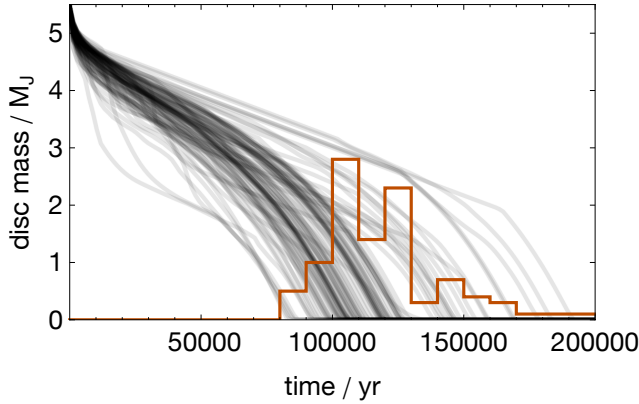


Figure 1. The evolution of the remaining disc mass for each run is plotted in gray. The red histogram shows the (arbitrarily normalized) distribution of dissipation times, i.e. when the disc mass reaches 0.

planet-disc interactions (Masset 2000). We have modified the code somewhat to make it more suitable for this work (similar modifications were made by Marzari et al. 2010). The n -body integrator was changed from a 5th order Runge-Kutta to a (7,8) order embedded pair (Prince & Dormand 1981). We include stepsize control in the following way: the results of the 7th and 8th order estimate of each component of each planet’s velocity and position are compared at the end of each hydrodynamic timestep. If the fractional difference between the two exceeds 10^{-7} , the planets are integrated through the hydrodynamic step with a smaller n -body timestep, repeating this process until our accuracy criterion is met.

We have also implemented the removal of escaping planets if they are on a hyperbolic orbit and more than 400 au from the star, as well as collisions between planets and between planets and the star. Planet–planet mergers are mass and momentum conserving and take place whenever two planets’ surfaces are detected to touch, with all planets assumed to have radii of $1.3 R_J$. Planets merge with the star if they approach within $5 R_\odot$.

2.2 Numerical details

Photoevaporation is included using the X-ray driven mass-loss profile of Owen et al. (2011), scaled to our $1 M_\odot$ star and chosen X-ray luminosity of 1.4×10^{30} erg s^{-1} . The azimuthally constant but radially dependent mass loss rate from these profiles is imposed across the numerical grid as an externally specified sink term in the continuity equation. In these models photoevaporation opens a gap near 2 au, and when the gas interior to the gap is gone the directly-illuminated outer disc erodes from the inside out (see Figure 9 of Owen et al. 2011). We implement this transition to direct illumination somewhat approximately, as we do not follow the disc inwards of 1 au and set a lower surface density limit of 2×10^{-3} g cm^{-2} below which we do not photoevapo-

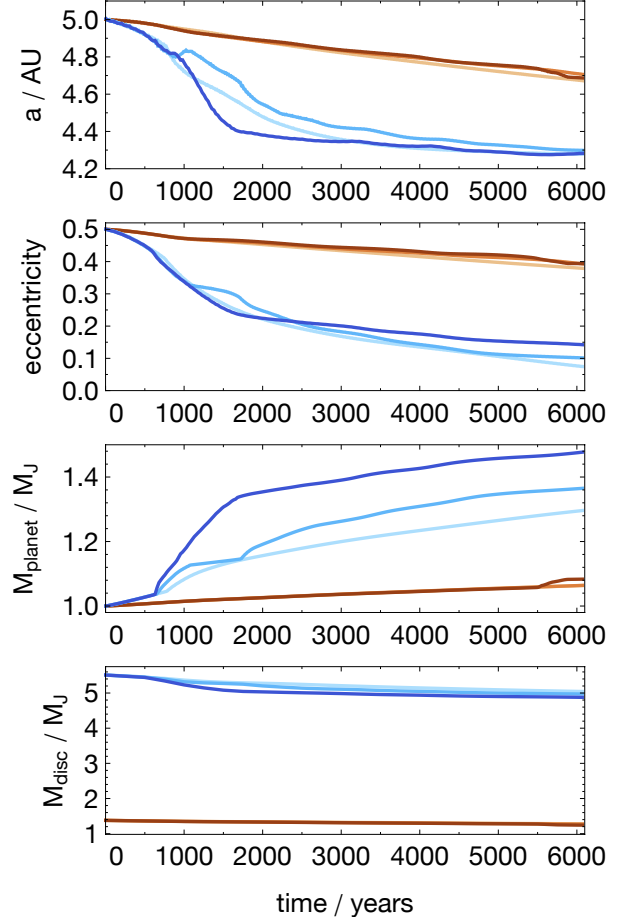


Figure 2. Resolution tests in which a $1 M_J$ planet is placed on an eccentric orbit in an initially unperturbed disc. The series of blue lines shows a disc with $\Sigma(1 \text{ au}) = 200 \text{ g cm}^{-2}$, and the red lines have $\Sigma(1 \text{ au}) = 50 \text{ g cm}^{-2}$. In each series the lightest shade is run with $n_\theta = 256$, the medium shade with $n_\theta = 512$, and the dark shade with $n_\theta = 1024$.

rate any material for numerical reasons². As the simulation progresses, we track the azimuthally averaged surface density of each ring. When the innermost radius has an average surface density below 8×10^{-3} g cm^{-2} , we rescale the inner radius of the photoevaporation profile to that radius.

We allow accretion onto the planets using a similar approach to the unmodified version of FARGO, based on the prescription used by Kley (1999). The planet’s Roche lobe (approximated by a constant radius R_r) is drained on some timescale, with material inside $0.45 R_r$ drained at twice the rate of that between 0.45 and $0.75 R_r$. Material outside $0.75 R_r$ is left alone. The timescale on which the Roche lobe is drained is set to twice the planet’s orbital period. With our chosen parameters, the disc is typically dispersed via a combination of planetary dynamics and photoevaporation (with a small contribution from accretion) between 1 – 1.5×10^5 yr, with a few instances stretching to 0.8 – 1.9×10^5 yr. In Figure 1 we show the mass evolution of all the discs in our runs.

² With this density floor, our final disc mass when photoevaporation has run its course is $\sim 10^{-3} M_J$.

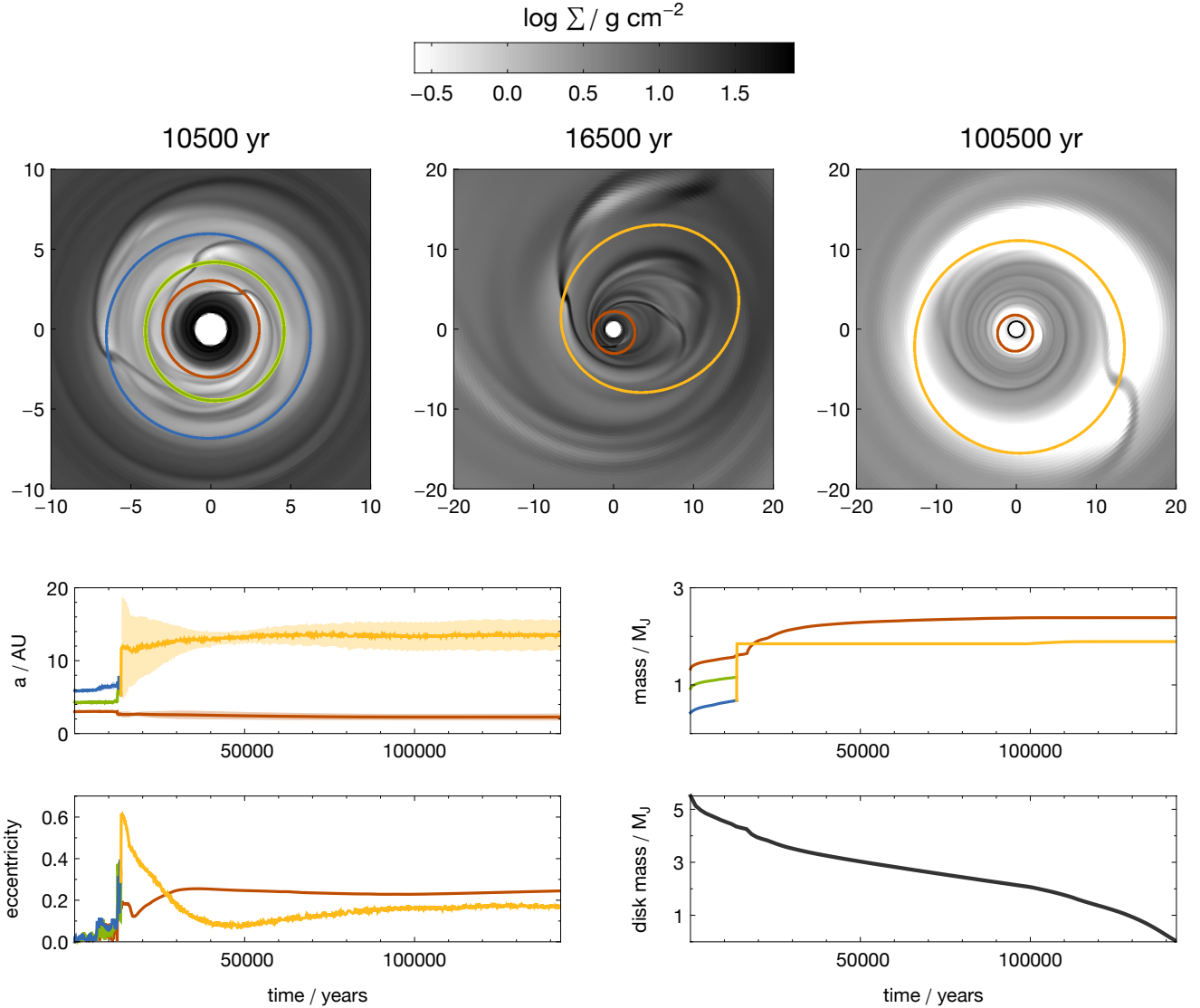


Figure 3. The evolution of the planetary system and the gas disc for an example run. The orbits of the planets are plotted on top of the surface density plots in the same colours as the plots of the orbital elements and masses. The surface density plot on the left shows the system before scattering, when the red, green, and blue planets have partially cleared a mutual gap. During the scattering event the green and blue planets collide to form the orange planet on an orbit with $e \sim 0.6$. The aftermath of the scattering is shown in the middle density plot. Over the next $\sim 2.5 \times 10^4$ years, disc interactions damp the eccentricity of the outer planet; after disc clearing, the two planets are stable. The right density plot shows the system near the end of the photoevaporative clearing, with each planet orbiting in a gap.

We use open boundaries at the inner and outer edges of the grid. We use a fixed disc aspect ratio of $H/r = 0.04$, and an alpha-viscosity with $\alpha = 10^{-2}$. The grid is setup with $n_\theta = 512$ azimuthal cells, and $n_r = 207$ rings. The radial spacing is logarithmic, with approximately square cells between 2.5 and 10 au, but coarser radial spacing between 1–2.5 and 10–40 au so that those cells are rectangular with a 2:1 aspect ratio. Our highest resolution is thus concentrated in the region of highest interest, where the majority of the planets spend most of the time.

We tested the adequacy of the grid resolution by setting up a planet with $m = 1 M_J$, and eccentricity $e = 0.5$, in an initially unperturbed disc. We considered two initial disc

masses, $\Sigma(1 \text{ au}) = 200$ and 50 g cm^{-2} , and three resolutions, $n_\theta = 256, 512$, and 1024 . The results are shown in Figure 2. The more massive disc results are shown in blue, and the low mass disc in red. The lightest shade is $n_\theta = 256$, and the darkest shade is $n_\theta = 1024$. The low mass disc is well converged in both the orbital evolution and planet mass. The high mass case is only moderately converged. While the orbit of the planet ends up at approximately the same place for all three resolutions, the mass evolution of the planet is quite different. The differences in the orbital evolution are most pronounced at the time when the planet is accreting the most mass, between 1000–2000 yr. Visual inspection of the surface density of these runs shows that gas is accreting

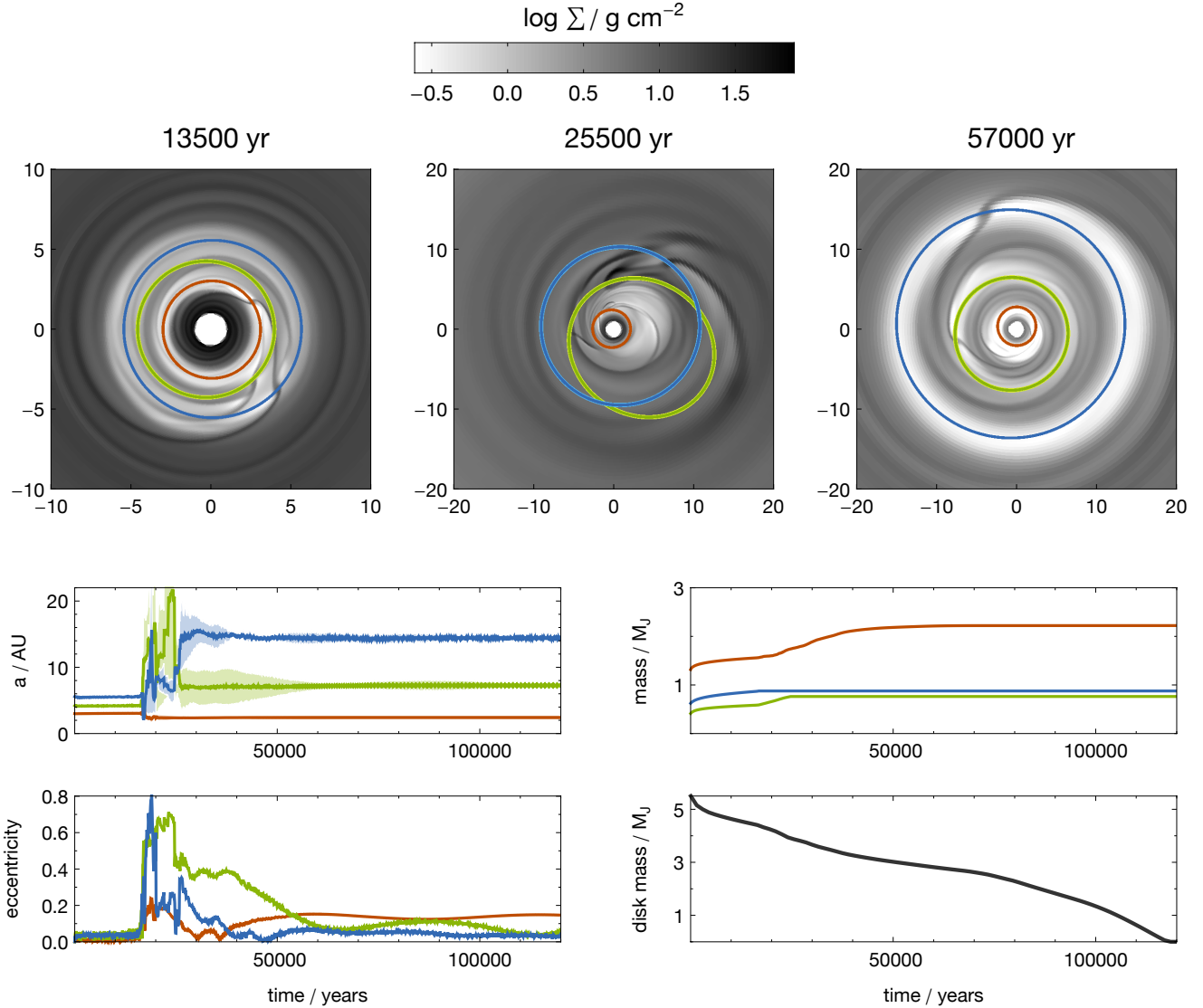


Figure 4. The evolution of the planetary system and the gas disc for an example run. The orbits of the planets are plotted on top of the surface density plots in the same colours as the plots of the orbital elements and masses. The surface density plot on the left shows the system before scattering, when the red, green, and blue planets have partially cleared a mutual gap. The middle density plot is during a period of active planetary dynamics. After this stage the disc damps the eccentricity of the three planets, which remain in roughly this configuration through 10^8 yr. This phase is shown in the right density plot.

onto the planet in streams that are not well resolved at low n_θ . We conclude that for studying the orbital evolution of the planets — the prime focus of this work — $n_\theta = 512$ is sufficient. Higher resolution, along with a more physical treatment of mass accretion within the Roche lobe, would likely be needed to model mass evolution in detail.

The results of the resolution test suggest that a massive planet scattering into an undisturbed disc will accrete material at a resolution-dependent rate until a gap is opened. This manifests itself as an offset in the mass evolution of the disc and the planet (see the similar slopes of the M_{planet} and M_{disc} curves in Figure 2 after ~ 1500 years). Runs that scatter very early, when a large amount of gas is still in the disc, are susceptible to this numerical effect, which may alter the disc dissipation timescale. Offsets of the order $0.1 M_J$ will

not move the disc mass evolution out of the main band seen in Figure 1 though, and are certainly small compared to the expected physical dispersion in dissipation history that results from varying stellar X-ray luminosity. Hence, we do not consider this to be of great importance.

Each set of initial conditions is integrated with FARGO until the disc is photoevaporated down to our density floor, at which point the run is terminated. The planetary system is then evolved further using the FARGO integrator with no disc until 2×10^5 yr. At this point, the system is turned over to the Burlisch-Stoer integrator of MERCURY (Chambers 1999) and integrated to 50 Myr. As in the FARGO portion of the integration, planetary mergers and ejections are allowed with the same parameters. These hydrodynamic runs are then compared to an ensemble of 500 purely n -

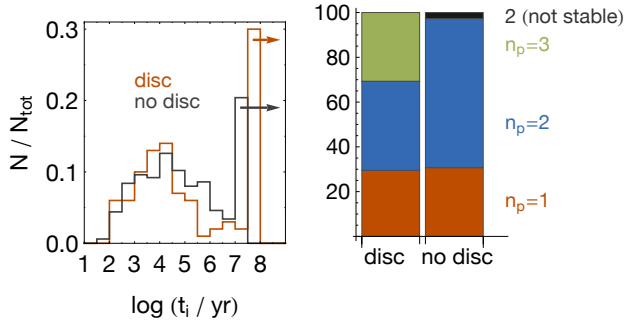


Figure 5. *Left:* The distribution of the instability times for the runs with a disc (red) and without (black). The final bins include all runs still stable at 50 Myr for the disc runs, and 15 Myr for the discless runs. *Right:* The final state of the planetary systems after 50 Myr (for the disc runs) and 15 Myr (for the discless runs). The bins labeled ‘ $n_p = 1$ ’ and ‘ $n_p = 2$ ’ refer to single planet systems and double systems that are formally Hill stable. The bin labeled ‘2 (not stable)’ refers to 2 planet systems that are not Hill stable. Triple planet systems (‘ $n_p = 3$ ’) include only those that underwent a scattering event but retain three planets at the end of the simulation.

body simulations, set up using identical initial conditions but integrated using MERCURY throughout.

3 RESULTS

The hydrodynamic runs are characterised by several phases: an initial clearing of gaps and relaxation of the disc, the onset (or not) of dynamical instability and planet scattering, renewed relaxation of the disc and eccentricity damping, and clearing of the disc by photoevaporation. These phases are illustrated for two example runs in Figures 3 and 4. In each of these examples scattering occurs, and the once-prominent gaps are filled in. As the disc comes to terms with the new planetary configuration eccentric gaps develop (also noted by Marzari et al. 2010), and finally the disc is cleared leading to the purely gravitational phase of our experiments. Here we discuss the most interesting aspects of these simulations.

3.1 Instability timescale and outcome

In Figure 5 we compare the distribution of instability times between the hydrodynamic and n -body control runs. During the FARGO runs, the time of scattering is identified as the first time the semi-major axis of any planet changes by 10 percent between two output times. Visual inspection of the results confirms that this is a reasonable estimate of the onset of instability. During the MERCURY runs, an encounter between two planets within 3 Hill radii is the criterion. The bulk of the distribution is similar for both sets of simulations; the main difference is at the long-time tail of the distribution, where the FARGO runs have roughly 50% more runs that never go unstable over the course of the simulations.

In the right panel of the figure we plot the percentage of unstable runs ending in a given planetary configuration. The main difference between the simulation sets is the number of unscattered systems and the presence, in the hydrodynamic runs only, of a population of scattered systems that retain

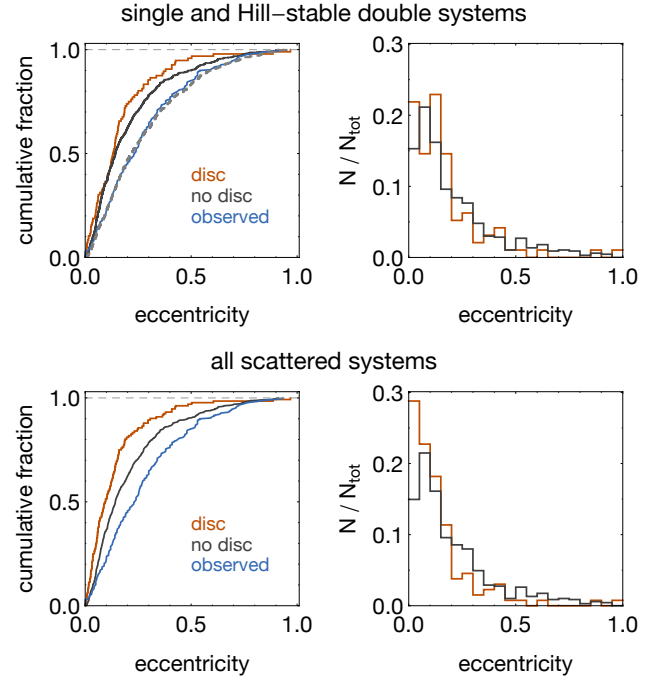


Figure 6. The eccentricity distribution at 10^8 yr for observed exoplanets (blue), the runs with no disc (black), and the runs with a disc (red). The dashed line shows the disc-less result with random inclinations up to 1° . Top panels show only single and Hill stable double systems: K–S and A–D tests do not conclusively rule out the null hypothesis that the latter two distributions are the same (p-values 0.10 and 0.037, respectively). Bottom panels include all systems that scattered prior to 50 Myr, i.e. including triples and non Hill stable doubles. K–S and A–D tests reject the null hypothesis for these samples (p-values $< 10^{-3}$).

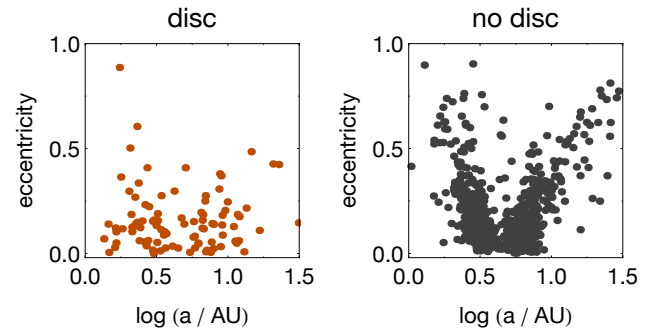


Figure 7. Semi-major axis–eccentricity scatter plots of the stable systems at 10^8 yr with and without the disc. A two-dimensional K–S test rejects the null hypothesis that the two distributions are the same (p-value 0.041).

all three planets. There are also a handful of double systems that are not provably Hill stable in the MERCURY runs, but not enough to alter any conclusions. We discuss the difference in the percentage of unscattered triple systems further in sections 3.3 and 3.4.

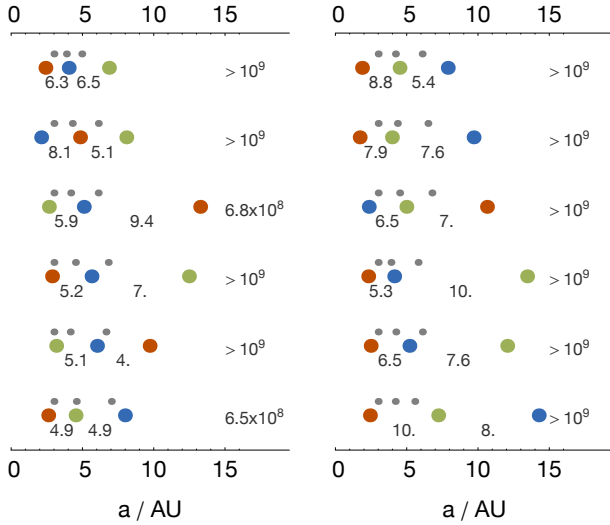


Figure 8. The spacings of the triple systems in the disc runs (the ' $n_p = 3$ ' bin in Figure 5). Each row shows one system: small grey points show the initial spacing of the planets, and the large coloured points show the semi-major axes at 50 Myr. The colours correspond to the initial ordering: red points were originally the innermost planet, green points were in the middle, and blue points were outermost. The numbers between adjacent points show how many symmetric Hill radii separate the pair. The number to the right of each set shows the scattering time taken from extended runs to 10^9 yr; only two systems went unstable in that time.

3.2 Eccentricity distributions

With realistic planet masses, scattering from nearly (but *not* identically) coplanar and circular initial conditions is quite successful at reproducing the observed eccentricity distribution of giant extrasolar planets. Good agreement can be obtained irrespective of the initial number of planets (Ford & Rasio 2008; Chatterjee et al. 2008; Jurić & Tremaine 2008). These authors compare their results to the observed sample³. In our study, a subtlety arises from the fact that FARGO is a 2D code, and thus we simulate the planetary dynamics strictly in the plane. This has some consequences for the eccentricity distribution obtained by purely gravitational studies; namely, the distribution is shifted toward lower eccentricities, clearly seen in Figure 6. We address this point further in appendix A. When comparing our FARGO runs to a disc-less n -body result we thus compare to a coplanar suite of experiments run with MERCURY rather than directly to the observed sample. With non-zero inclinations, these initial conditions yield a distribution quite close to the observed exoplanets in a pure n -body suite of experiments, which we verify by running the same initial conditions with random inclinations up to 1 degree. For the observed sample we exclude exoplanets with $a < 0.1$ au to take tidal circularisation out of consideration.

To statistically compare the sets of simulations we perform two-sample Kolmogorov–Smirnov (K–S) tests and two-sample Anderson–Darling (A–D) tests on the cumulative distributions. The latter test is more sensitive to deviations

³ Available from <http://exoplanet.eu>.

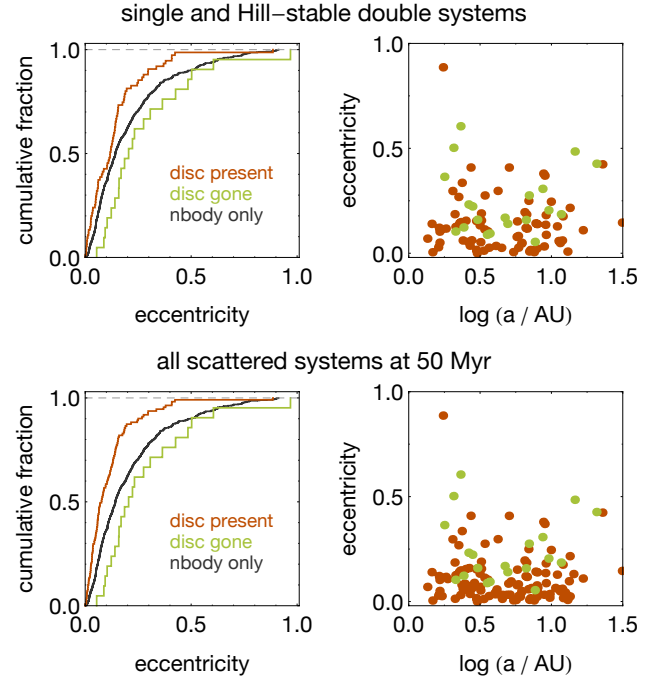


Figure 9. The eccentricity distribution of stable systems (top) and all scattered systems (bottom), with the runs with discs divided into those that scattered with disc material present and those that scattered after disc dispersal. K–S and A–D tests reject the null hypotheses that the early scatterers follow the same distribution as the late scatterers (p-values 0.0016 and 3.2×10^{-4}) or the disc-less runs (p-values 0.0069 and 6.6×10^{-4}). The late scatterers are ambiguously distinct from the disc-less runs (p-values 0.067 and 0.033). Two-dimensional K–S tests on the semi-major axis–eccentricity distributions of the early and late scatterers likewise reject the null hypothesis only when unstable systems are included (p-value 0.071 with only stable systems, 0.0037 with unstable systems).

at the tails of the distribution. We reject the null hypothesis that the two samples are drawn from the same distribution when p-values are less than 0.05. In Figure 6 we show the eccentricity distributions of the disc and disc-less cases. The top panels show the results including only those systems that are provably stable, i.e. single planet and Hill-stable double planet systems. The null hypothesis is not ruled out by the K–S (p-value = 0.10), though the A–D test rejects it (p-value = 0.037). The greater weight the A–D test gives to the distributions' tails validates the visual impression that the main difference is at the high eccentricity end. For comparison we also plot the observed eccentricity distribution, as well as the result of our simulations with inclinations up to 1 degree. While the eccentricity distributions alone are quite similar for stable systems, the combined eccentricity–semi-major axis distribution is marginally different. Figure 7 shows scatter plots of these distributions. A 2D K–S test (using the method in Fasano & Franceschini 1987) rejects the null hypothesis, with a p-value of 0.041.

The bottom panel of Figure 6 shows the same comparison between the hydrodynamic and n -body integrations, but now including all systems that scattered prior to 50 Myr, regardless of provable stability. This means that for the FARGO runs we include those triples that scattered and

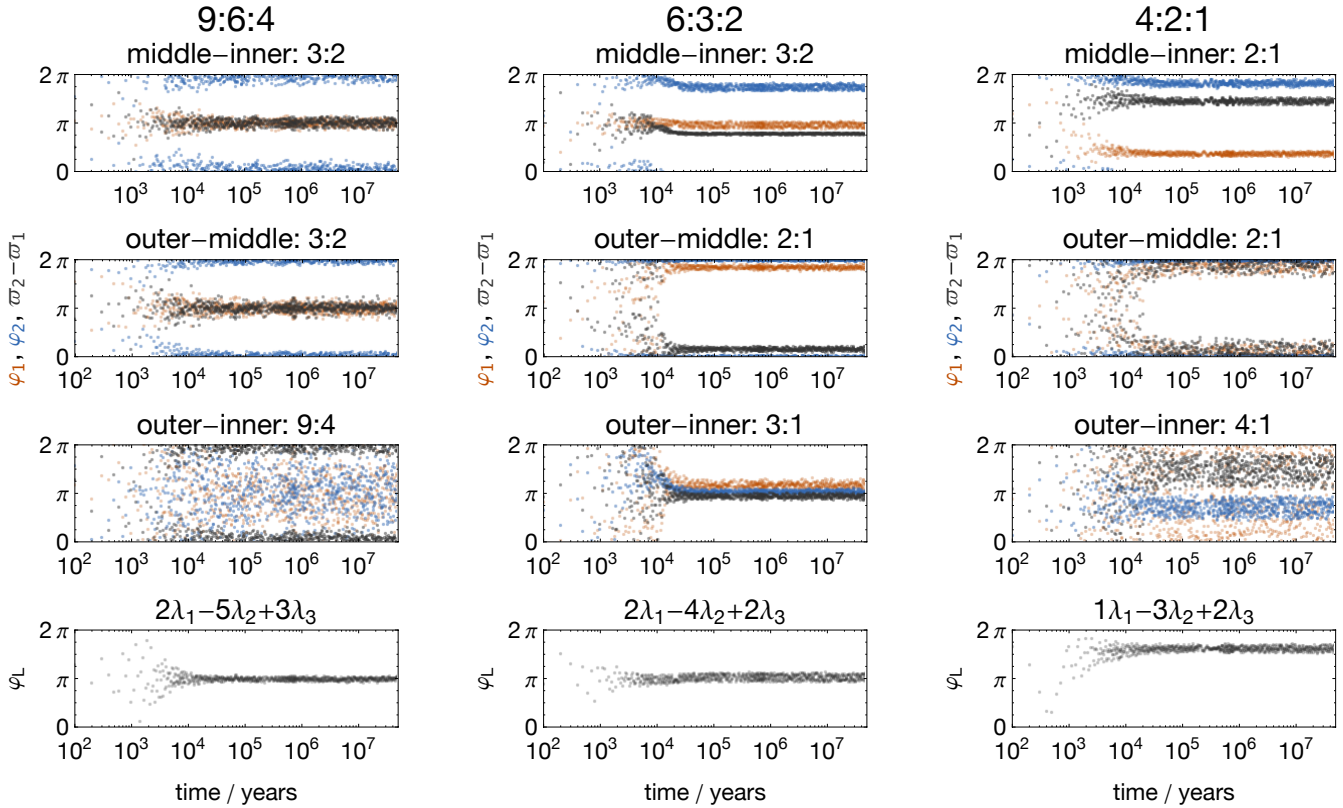


Figure 10. The evolution of the planetary system and the gas disc for an example run. The orbits of the planets are plotted on top of the surface density plots in the same colours as the plots of the orbital elements and masses. The surface density plot on the left shows the system before scattering, when the red, green, and blue planets have partially cleared a mutual gap. During the scattering event the green and blue planets collide to form the yellow planet on an orbit with $e \sim 0.6$. The aftermath of the scattering is shown in the middle density plot. Over the next $\sim 2.5 \times 10^4$ years, disc interactions damp the eccentricity of the outer planet; after disc clearing, the two planets are stable. The right density plot shows the system near the end of the photoevaporative clearing, with each planet orbiting in a gap.

re-circularised in more widely spaced configurations (such as the one in Figure 4), while for the MERCURY runs we include the few double systems that are not provably stable. These distributions are visually more distinct, and this is born out by the statistical tests, with p-values for both tests less than 10^{-3} . To test that the scattered triples are stable on longer timescales, we integrated the 12 cases further⁴, to 10^9 yr. The spacing of these systems at 50 Myr, and the outcome of the further integration, are shown in Figure 8. With two exceptions, the systems remain stable for 10^9 yr.

Since the disc is the driver of any difference that might arise between the distributions, we split the sample into those in which instability begins when disc material is still present, and later scatterers. These distributions are shown in Figure 9. Whether or not we include the unstable systems, the distribution of early and late scatterers are significantly different, with K–S and A–D p-values of 0.0016 and 3.2×10^{-4} . While the early scatterers are likewise convincingly statistically distinct from the disc-less runs (p-values 0.0069 and 6.6×10^{-4}), the two tests also ambiguously reject the null hypothesis for the disc-less runs and the late scatterers (p-values 0.067 and 0.033). We would not necessarily

expect any difference here, as there is no disc to alter the dynamics, and Chatterjee et al. (2008) showed that the time of instability is unimportant in determining the final outcome of a scattering experiment. Note that we suffer somewhat from low numbers of runs in this late scattering category, due to the large number of runs that never scatter over the length of our integrations.

3.3 Mean Motion Resonances: 2 planets

Convergent migration in a disc can lead to trapping into resonance (e.g. Lee & Peale 2002; Snellgrove et al. 2001; Kley et al. 2004; Moorhead & Adams 2005), and is seen with high frequency in the previous work most relevant to this one, the coupled n -body –1D disc models of Matsumura et al. (2010). We first searched for mean motion resonances (MMRs) among the 39 stable double systems by observing the apsidal alignment $\varpi_2 - \varpi_1$ and the resonance angles for a $(p + q) : q$ MMR given by (e.g. Murray & Dermott 1999)

$$\varphi_{1,2} = (p + q)\lambda_2 - p\lambda_1 - q\varpi_{1,2}. \quad (2)$$

Here subscript 1 and 2 refer to the inner and outer planet, λ is the mean longitude, and ϖ the longitude of pericenter. We searched for resonances up to 8th order by monitoring these angles for libration around fixed values.

⁴ For these integrations we used the Hybrid integrator of MERCURY, with a 20 day stepsize.

We find just two double systems in 3:1 MMRs with libration semi-amplitudes of ~ 150 and $\sim 80^\circ$. The case with the larger libration amplitude did not scatter until the disc had been photoevaporated. The low frequency of 2 planet resonances, and the large libration angles, are symptomatic of random entry into resonance due to purely gravitational effects (Raymond et al. 2008), rather than systematic driving into resonance due to gas disc migration (Matsumura et al. 2010). We observe a dramatically lower resonant fraction than the ~ 75 percent seen by Matsumura et al. (2010). The difference is probably due to the short lifetime of the discs in this study compared to the Myr dispersal timescales assumed by Matsumura et al. (2010), which allows less time for post-scattering migration to move planets into resonance.

As noted in section 3.1, the disc runs have a higher fraction that remain stable for the entire simulation than the n -body only runs. Because our initial conditions naturally place the planets near to several MMRs, there is the possibility that two adjacent planets may get trapped into resonance, a situation that can enhance the stability of a three planet system (Fabrycky & Murray-Clay 2010). We also search each adjacent pair of planets in the systems that never scattered for MMRs. Out of 27 such cases, we find three in which the inner two planets are in resonance (two 3:2 and one 2:1), and three cases in which the outer two planets are in a 2:1 resonance. These resonant systems are potentially part of the reason for the large number of unscattered systems.

3.4 Mean Motion Resonances: 3 planet resonant chains

Further investigating the unscattered runs, we discovered that 12 of the 27 unscattered runs are in three body resonance. In eight cases the inner–middle and middle–outer pair move into resonance with librating resonance angles (equation 2), and in three of these the inner–outer pair are likewise in a resonance. The chains we find are 9:6:4 (four cases), 6:3:2, 3:2:1 (two cases), and 4:2:1⁵. In each case a Laplace angle of the form

$$\varphi_L = m\lambda_1 - (m+n)\lambda_2 + n\lambda_3 \quad (3)$$

is identified (Aksnes 1988), which librates around a fixed value for small integer values of m and n , with subscripts 1,2,3 referring to the inner, middle, and outer planets.

The other four of the 12 triple resonances are less deeply in resonance; all three exhibit libration of the $m = 1$, $n = 3$ Laplace angle but the adjacent planet pairs are not in the 2:1 resonances. In Figure 10 we plot the resonant behavior of three example chains; a representative of the 9:6:4 cases (i.e. a double 3:2 resonance), the 6:3:2 case, and the Laplace resonance case, the former two of which exhibit asymmetrical resonance in some of the angles. In the 9:6:4 run each adjacent pair of planets is trapped into a 3:2 resonance at ~ 4000 yr, the same time that the Laplace angle begins librating around $\varphi_L = \pi$. The inner–outer pair move into apsidal alignment, but the resonant angles continue to circulate.

⁵ The Laplace resonance, as seen in GJ 876 (Rivera et al. 2010) and potentially HD 82943 (Beaugé et al. 2008).

The 6:3:2 case moves into triple resonance at ~ 1000 yr, roughly the same time as the inner–middle pair lock into a 3:2 resonance, but somewhat before the other two pairings fully enter resonance at $\sim 10^4$ yr. The initial inner–middle resonance and the Laplace angle all appear to be settling toward resonant angles of 0 or π , but when middle–outer and inner–outer resonance begin, most of the angles move into asymmetrical resonances, including the Laplace angle which shifts to librate around a value (very) slightly more than π .

The double 2:1 Laplace resonance shows libration of φ_L around an angle completely incommensurate with π . In this case the inner–middle 2:1 pair immediately enters asymmetrical resonance, along with the Laplace angle. The middle–outer 2:1 pair are in a symmetric resonance, and the inner–outer pair are flirting with asymmetric resonance, though ϕ_1 continues to circulate. We note that this asymmetric behavior in the Laplace resonance is a preferred outcome of simulations of migration into double resonance (Beaugé et al. 2008), although this particular case did not undergo very much migration. It would appear that the high incidence of triple resonances, as well as the perhaps enhanced stability due to a single adjacent pair migrating into resonance, are the underlying reason behind the large number of unscattered systems in our hydrodynamic simulations compared to the n -body runs.

3.5 Periods of observability

Disc-planet interactions may be able to excite eccentricity to modest values, $e \sim 0.1$ – 0.2 (D’Angelo et al. 2006), but planetary dynamics are probably necessary to reach higher values. Some of the more interesting features in the disc surface density in our simulations occur when eccentricities are high, during or just after scattering (see Figures 3 and 4). These include non-axisymmetric features, new gaps being opened, and eccentric gaps. If scattering (or at least its signature in the eccentricity of the planets) is reasonably common in transitional discs, then these features may be observable. We estimate the likelihood that these features might be observed by calculating the amount of time that systems spend with at least one planet’s eccentricity above a threshold value, while also having at least 1 M_J of gas left. This distribution is shown in Figure 11 for three values of the threshold eccentricity, $e_{min} = 0.1, 0.25,$ and 0.5 .

For the higher and more interesting thresholds, most of the runs do not have eccentric enough planets for any reasonable amount of time. If we require that interesting features are present for something like 25% of our typical disc lifetime, $t_{obs} \sim 3 \times 10^4$ yr, a threshold of $e_{min} = 0.25$ means that 10–15% of the runs will have planets in eccentric enough orbits to be noticeable; thus a few percent of transition discs might be expected to harbor planets caught in the act or the aftermath of scattering.

4 CONCLUSIONS

If planets exit the gas disc phase in non-resonant configurations, a significant fraction of unstable systems are likely to scatter roughly contemporaneously with the transition between gas-rich and gas-poor conditions. We have studied

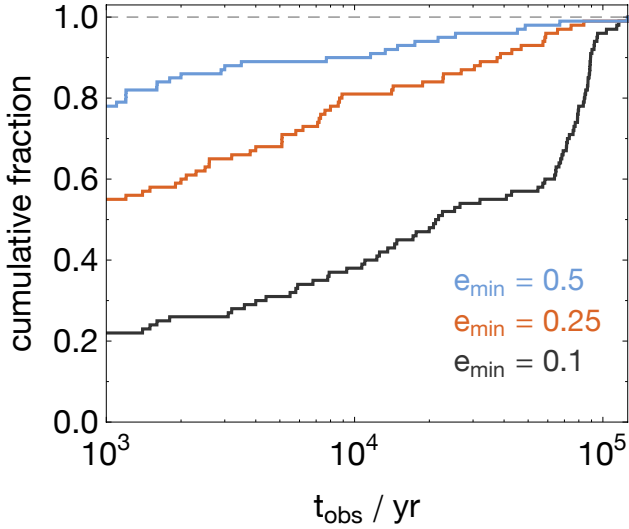


Figure 11. The cumulative distribution of t_{obs} , defined as the amount of time a system with at least $1 M_J$ of gas left in the disc harbors at least one planet with $e > e_{min}$.

whether the presence of small masses of gas, in photoevaporating transition discs, significantly modifies the outcome of scattering. Previous work that has addressed this question has been ambiguous. Detailed statistical studies, using approximate hydrodynamic treatments of the disc, have suggested that gas free initial conditions are a reasonable approximation to the more physically complete case that includes gas (Chatterjee et al. 2008; Matsumura et al. 2010). On the other hand, earlier hydrodynamical work suggested a possibly significant effect (Moeckel et al. 2008; Marzari et al. 2010), but was hampered by very limited statistics. The immediate aftermath of a scattering event, when multiple gravitationally interacting planets can have high-eccentricity orbits that take them into previously undisturbed regions of the disc, is clearly the most challenging situation to model reliably with simple prescriptions. As shown, for example, in Figure 3, these phases can be important in shaping the long-term evolution of scattered systems, though such individual examples do not mean that the statistical results obtained from a damping prescription might not be “good enough”. Here, we have presented results from a direct hydrodynamic simulation of a moderately large ensemble of systems, which we have used to extract statistical results for the eccentricity distribution and for the abundance of resonant planetary configuration. We find some differences between our hydrodynamic results and previously published results derived using approximate methods, though we defer for future work the question of whether *other* analytic prescriptions for planet-disc interactions would yield better agreement.

Our main result is that scattering of random three-planet systems, from non-resonant initial conditions, yields significantly lower eccentricities (as compared to n -body runs) when the effects of hydrodynamics are included. This difference does *not*, however, arise because of any major change in the dynamics of scattering events that either eject planets, or result in planetary mergers. In these —

dominant — channels, scattering in the hydrodynamic and n -body simulations leads to statistically very similar eccentricity distributions, differing (if at all) only in the fraction of highly eccentric planets. Rather, the lower eccentricities found in the hydrodynamic case occur because a modest number of scattering events evolve into three planet systems that appear to be stable over an observationally interesting time scale (at least a Gyr). These systems, which tend to have lower than average eccentricities, are simply not present in runs without gas, whose end state after scattering is uniformly either one or two planet systems.

Despite the lower eccentricities, we interpret our results as supporting the model of planetary scattering as the dominant physical mechanism giving rise to observed exoplanet eccentricity. Although gas does impact the outcome of scattering, it does not lead to large-scale circularization of planetary orbits. The differences between the hydrodynamic and gas-free simulations, in fact, are comparable to the variations seen in scattering simulations that start with different planetary mass functions (Raymond et al. 2010). It would almost certainly be possible to find some set of plausible initial conditions that would evolve hydrodynamically, under scattering, to match the observed distribution of massive planet eccentricity, given the freedom to fine tune the initial planetary spacing or disc dispersal time. Alternatively, and perhaps more naturally, the fraction of stable triple planet systems that are responsible for the lower eccentricity could likely be suppressed by starting with $n_p > 3$. Given the wealth of such possibilities, our results do not constitute an argument against the physical importance of scattering, though they do imply that the relatively precise agreement between n -body calculations and observations is likely fortuitous.

The frequency of resonant systems of multiple planets is potentially a much more sensitive probe than the eccentricity distribution of the physics predating scattering. Under purely gravitational evolution, the occupation fraction of resonant systems mirrors the available phase space, and MMRs are uncommon (a few percent, Raymond et al. 2008). In a laminar, viscous disc, conversely, almost arbitrarily high resonant fractions can be achieved (Matsumura et al. 2010). Our results fall somewhere in between these extremes. The frequency of 2-planet resonances that we find is comparable to that found in pure n -body simulations. This is consistent with the conclusion, noted above, that the hydrodynamics and dynamics of scattering are very similar for those channels that result in planetary ejection or merger. However, we also observe a high frequency of resonant chains of 3-planet systems. Out of 100 runs, 12 evolved into libration of the Laplace angle φ_L . This resonance trapping stabilized the systems against instability, pushing the number of unscattered systems in our runs to nearly 30%. Similar effects were seen in the n -body simulations of Raymond et al. (2010), where the dissipative role that is here played by gas was instead furnished by planetesimals. Observationally, some resonant systems are seen, but it is reasonably clear that their number is lower than theoretical expectations based on an extended period of evolution in a viscous disc. One possibility is that survival in resonance is frustrated at early times, when the disc is massive and turbulent fluctuations lead to stochastic torques on planets (Adams et al. 2008), such that resonance capture only becomes possible in a lim-

ited window just prior to disc dispersal. The quantitative details of such a scenario are, however, poorly known, and it is likely that our limited understanding of the mechanisms that can *disrupt* resonances is the dominant uncertainty in current models of early planetary system evolution.

Finally we have explored the potential of future imaging to directly observe the disc structures formed during the epoch of planetary scattering, which include eccentric gaps and massive planets directly accreting from the disc gas. The predicted structures are distinctive, but the limited synchronization between the onset of scattering and the dispersal of the disc means that they should only rarely be present in a sample of transition discs. We estimate an abundance that might be of the order of a few percent. A blind search of transition discs is thus unlikely to uncover any systems with ongoing scattering, though in principle it may be possible to exploit the large-scale asymmetries generated during scattering to identify possible candidates.

ACKNOWLEDGMENTS

Our thanks to the referee for a quick and constructive report. This work was performed in part using the Darwin Supercomputer of the University of Cambridge High Performance Computing Service (<http://www.hpc.cam.ac.uk/>), provided by Dell Inc. using Strategic Research Infrastructure Funding from the Higher Education Funding Council for England. PJA acknowledges support from NASA, under award NNX09AB90G and NNX11AE12G from the Origins of Solar Systems and Astrophysics Theory programs, and from the NSF under award AST-0807471.

REFERENCES

- Adams F. C., Laughlin G., 2003, *Icarus*, 163, 290
 Adams F. C., Laughlin G., Bloch A. M., 2008, *ApJ*, 683, 1117
 Aksnes K., 1988, in A. D. Roy ed., *Long-term Dynamical Behaviour of Natural and Artificial N-body Systems*. General formulas for three-body resonances.. pp 125–139
 Beaugé C., Giuppone C. A., Ferraz-Mello S., Michtchenko T. A., 2008, *MNRAS*, 385, 2151
 Butler R. P., Wright J. T., Marcy G. W., Fischer D. A., Vogt S. S., Tinney C. G., Jones H. R. A., Carter B. D., Johnson J. A., McCarthy C., Penny A. J., 2006, *ApJ*, 646, 505
 Chambers J. E., 1999, *MNRAS*, 304, 793
 Chambers J. E., Wetherill G. W., Boss A. P., 1996, *Icarus*, 119, 261
 Chatterjee S., Ford E. B., Matsumura S., Rasio F. A., 2008, *ApJ*, 686, 580
 D’Angelo G., Lubow S. H., Bate M. R., 2006, *ApJ*, 652, 1698
 Fabrycky D. C., Murray-Clay R. A., 2010, *ApJ*, 710, 1408
 Fasano G., Franceschini A., 1987, *MNRAS*, 225, 155
 Ford E. B., Rasio F. A., 2008, *ApJ*, 686, 621
 Gladman B., 1993, *Icarus*, 106, 247
 Jurić M., Tremaine S., 2008, *ApJ*, 686, 603
 Kley W., 1999, *MNRAS*, 303, 696
 Kley W., Peitz J., Bryden G., 2004, *A&A*, 414, 735
 Lee A. T., Thommes E. W., Rasio F. A., 2009, *ApJ*, 691, 1684
 Lee M. H., Peale S. J., 2002, *ApJ*, 567, 596
 Lin D. N. C., Ida S., 1997, *ApJ*, 477, 781
 Lubow S. H., Ogilvie G. I., 2001, *ApJ*, 560, 997
 Lubow S. H., Pringle J. E., 2010, *MNRAS*, 402, L6
 Marchal C., Bozis G., 1982, *Celestial Mechanics*, 26, 311
 Marzari F., Baruteau C., Scholl H., 2010, *A&A*, 514, L4
 Marzari F., Nelson A. F., 2009, *ApJ*, 705, 1575
 Marzari F., Weidenschilling S. J., 2002, *Icarus*, 156, 570
 Masset F., 2000, *A&AS*, 141, 165
 Matsumura S., Thommes E. W., Chatterjee S., Rasio F. A., 2010, *ApJ*, 714, 194
 Moeckel N., Raymond S. N., Armitage P. J., 2008, *ApJ*, 688, 1361
 Moorhead A. V., Adams F. C., 2005, *Icarus*, 178, 517
 Murray C. D., Dermott S. F., 1999, *Solar system dynamics*
 Owen J. E., Ercolano B., Clarke C. J., 2011, *MNRAS*, 412, 13
 Owen J. E., Ercolano B., Clarke C. J., Alexander R. D., 2010, *MNRAS*, 401, 1415
 Prince P. J., Dormand J. R., 1981, *Journal of Computational and Applied Mathematics*, 7, 67
 Rasio F. A., Ford E. B., 1996, *Science*, 274, 954
 Raymond S. N., Armitage P. J., Gorelick N., 2010, *ApJ*, 711, 772
 Raymond S. N., Barnes R., Armitage P. J., Gorelick N., 2008, *ApJ*, 687, L107
 Rivera E. J., Laughlin G., Butler R. P., Vogt S. S., Haghighipour N., Meschiari S., 2010, *ApJ*, 719, 890
 Snellgrove M. D., Papaloizou J. C. B., Nelson R. P., 2001, *A&A*, 374, 1092
 Terquem C., Papaloizou J. C. B., 2000, *A&A*, 360, 1031
 Thommes E. W., Lissauer J. J., 2003, *ApJ*, 597, 566
 Weidenschilling S. J., Marzari F., 1996, *Nature*, 384, 619
 Wolk S. J., Walter F. M., 1996, *AJ*, 111, 2066

APPENDIX A: THE EFFECT OF ZERO-INCLINATION INITIAL CONDITIONS

The FARGO and MERCURY scattering calculations reported in this paper employ exactly planar planetary initial conditions. This is done for reasons of computational economy: 3-dimensional hydrodynamic simulations with the same in-plane resolution as the 2D runs would require around two orders of magnitude greater resources. For many purposes, moreover, assuming planarity is not a bad approximation. Prior *n*-body scattering calculations, run using the same mass distribution as ours, show that the median inclination of surviving planets is only $\approx 10^\circ$ (Raymond et al. 2010). This means that the initial phase of scattering typically involves inclinations $i \sim h/r$, or smaller, and accordingly we expect that any hydrodynamic interaction with the disc will be dominated by planar effects (eccentricity damping, accretion) rather than fully 3D ones (such as warp excitation). As noted in Section 3, however, the assumption of exact coplanarity does introduce a technical subtlety, since the final $f(e)$ that results from scattering in planar systems is not the same as that which results from otherwise identical initial conditions with a small (of the order of one degree) non-zero inclination. Because of this subtlety, we compare

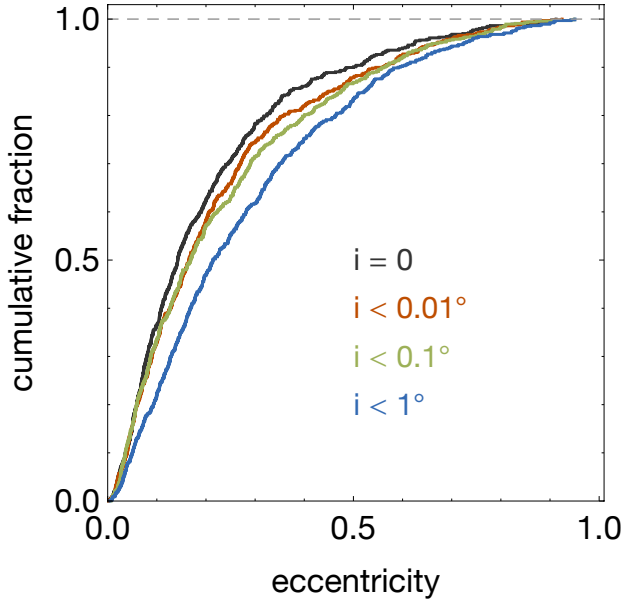


Figure A1. The cumulative eccentricity distributions, following scattering, obtained from purely n -body simulations of 3-planet systems initialized with different inclinations. The highest mean eccentricities result from initial conditions in which all three planets had inclinations chosen randomly and uniformly in the interval $i = [0, 1^\circ]$ (blue curve). Lower eccentricities result from choosing $i = [0, 0.1^\circ]$ (green), or $i = [0, 0.01^\circ]$ (red). The black curve shows results for a strictly planar geometry. In all cases, only surviving planets from those systems that went unstable during the integration are plotted.

our hydrodynamic simulations not to the same n -body runs that match the observed eccentricity distribution, but rather to their zero inclination analogues.

We emphasize that the point of this paper is not to argue that the result of the planar calculation is physically realistic. Rather, from the fact that in 2D the effect of hydrodynamics on the final eccentricity distribution is small, we infer that in 3D a hydrodynamic calculation would yield results similar to the observed distribution. That said, a physical effect is in principle possible if the gas disc were able to damp mutual inclinations (Lubow & Ogilvie 2001; Marzari & Nelson 2009) to the point where the final system was effectively planar. To quantify this possibility, we have run a set of n -body MERCURY experiments to identify how small the initial inclination must be for the system to scatter as if it were exactly planar. The setup is identical to that used earlier. We start with three planets on circular orbits, separated by $K = 4.0$ mutual Hill radii (Equation 1), with the inner planet at 3 AU. The mass spectrum is $f(m) \propto m^{-1.1}$ between $0.3 M_J$ and $5 M_J$, and the planetary radius is $1.3 R_J$. We run four ensembles of 500 simulations, with the planetary inclinations chosen randomly and uniformly in the range $i = [0, 1^\circ]$, $i = [0, 0.1^\circ]$, $i = [0, 0.01^\circ]$ and $i = 0$. The systems are integrated for 15 Myr, after which we plot the eccentricity distribution of the surviving planets in the unstable systems (at this epoch, this is about 80% of the total). As before, we discard double systems that are not Hill stable, which removes only ~ 10 runs from each set.

The results for the eccentricity distribution are shown in Figure A1. We find that the ensembles initialized with $i = [0, 0.1^\circ]$ and $i = [0, 0.01^\circ]$ are similar to, but statistically distinct from, the zero inclination limit (K–S p-values 0.049 and 0.023), whereas inclinations of the order of 1 degree are sufficient to result in markedly larger final eccentricities, distinct from all other distributions. To an order of magnitude, the condition for scattering behavior that is distinct from the 3D limit in these three planet systems is thus that the initial inclinations should satisfy $i < 0.1^\circ$.

Could real planetary systems be flat enough that their scattering dynamics are effectively two-dimensional? It seems unlikely. Although a gas disc damps the inclination of a single planet on a short time scale, it will damp the orbit until it is coincident with the local angular momentum vector of the gas, which will not be exactly constant with radius. A warp whose magnitude (over several AU) exceeds the threshold $\Delta i = 0.1^\circ$ seems almost inevitable (Terquem & Papaloizou 2000; Lubow & Pringle 2010). Even if the gas disc were perfectly flat, any temporary resonances between the planets would likely excite their mutual inclination (Thommes & Lissauer 2003) to the level where subsequent scattering would occur in the three-dimensional limit.

This paper has been typeset from a $\text{\TeX}/\text{\LaTeX}$ file prepared by the author.